

Design Rules for Tailoring Antireflection Properties of Hierarchical Optical Structures

Juan J. Diaz Leon, Anna M. Hiszpanski, Tiziana C. Bond, and Joshua D. Kuntz*

Hierarchical structures consisting of small sub-wavelength features stacked atop larger structures have been demonstrated as an effective means of reducing the reflectance of surfaces. However, optical devices require different antireflective properties depending on the application, and general unifying guidelines on hierarchical structures' design to attain a desired antireflection spectral response are still lacking. The type of reflectivity (diffuse, specular, or total/hemispherical) and its angular- and spectral-dependence are all dictated by the structural parameters. Through computational and experimental studies, guidelines have been devised to modify these various aspects of reflectivity across the solar spectrum by proper selection of the features of hierarchical structures. In this wavelength regime, micrometer-scale substructures dictate the long-wavelength spectral response and effectively reduce specular reflectance, whereas nanometer-scale substructures dictate primarily the visible wavelength spectral response and reduce diffuse reflectance. Coupling structures having these two length scales into hierarchical arrays impressively reduces surfaces' hemispherical reflectance across a broad spectrum of wavelengths and angles. Such hierarchical structures in silicon are demonstrated having an average total reflectance across the solar spectrum of 1.1% (average weighted reflectance of 1% in the 280–2500 nm range of the AM 1.5 G spectrum) and specular reflectance <1% even at angles of incidence as high as 67°.

1. Introduction

Most optical components utilize antireflective coatings based on multilayered destructive interference to reduce surfaces' reflectance. However, this principle of operation limits the efficacy of antireflective coatings to narrow wavelength ranges and angles of incidence. Thus, such antireflective coatings have only limited utility for many optical devices, like solar cells or photodetectors that require reduced reflectivity across broad wavelength regimes and angles of incidence. Furthermore, such antireflective

coatings work best at reducing specular reflectance, but depending on the application, a reduction in the diffuse or hemispherical (sum of the diffuse and specular) may instead be desired.

Because reflections occur whenever propagating light encounters a significant change in the index of refraction, an alternative antireflective approach is to create surfaces with a graded index of refraction. Such gradients can be simply created by texturing surfaces with structures so that the effective index of refraction varies from the tip to the base of the structure. High-aspect ratio wires with nanometer- or micrometer-scale diameters have been demonstrated as effective antireflective and light-trapping structures.^[1–11] However, such high-aspect structures are also fragile and challenging to reproducibly fabricate, which is problematic because the spectral response of such structures is highly sensitive to the exact tapering profile of nanowires.^[12–17]

Alternatively, hierarchical structures, which are composed of two or more substructures that have different characteristic length scales and are stacked atop one

another, have also been shown to effectively reduce reflectance. Because they do not require high aspect ratios to reduce reflectance, hierarchical structures can be easier to produce. Furthermore, while the two different substructures introduce more design variables, which can complicate optimization, they also provide further tunability over the reflective properties of hierarchically structured surfaces.

Though a number of hierarchical antireflective structures have been demonstrated,^[18–24] general guidelines for the design parameters of hierarchical structures to attain desired antireflective properties are still lacking. We explored the parameter space of hierarchical structures to synthesize a set of guidelines relating how their structural parameters affect various aspects of their reflectivity, including the type of reflectivity (e.g., specular, diffuse, hemispherical), its spectral response, and its angle-dependency, across the solar spectrum (250–2500 nm). Because of the UV–vis–IR spectral regime we are targeting, our hierarchical structures are composed of substructures on the nanometer- and micrometer-length scales that we refer to as “nanoarrays” and “microarrays,” respectively. We determine how combining nanoarrays and microarrays and tuning their

J. J. Diaz Leon, Dr. A. M. Hiszpanski, Dr. J. D. Kuntz
Materials Science Division
Lawrence Livermore National Laboratory
Livermore, CA 94551, USA
E-mail: kuntz2@llnl.gov

Dr. T. C. Bond
Materials Engineering Division
Lawrence Livermore National Laboratory
Livermore, CA 94551, USA

DOI: 10.1002/adom.201700080

dimensions and periodicity can affect the overall hierarchical structures' reflective response.

2. Results and Discussion

To understand the role of the micro- and nanometer length scale structures in reducing the reflectivity of hierarchical structures, we first studied the two length scale structures individually. In COMSOL, we modeled microarrays as triangles with a 5 μm base and height and modeled nanoarrays as yet smaller triangles that have a 100 nm base and 677 nm height.

To validate our computational results, we fabricated silicon microarrays, nanoarrays, and hierarchical structures that approximate our modeled structures by adapting previously described methods.^[18,19] Our fabricated structures consist of pyramids having comparable widths and heights of $\approx 5.2 \pm 3.3 \mu\text{m}$ and nanowires with heights of $\approx 625 \pm 122 \text{ nm}$ and widths varying between ≈ 50 and 200 nm, as shown in Figure 1. Briefly, to produce microarrays consisting of pyramids, we subjected (100) silicon wafers to KOH-etching, an often-used technique in the solar cell industry to reduce silicon's reflectance from $\approx 34\%$ to $\approx 10\%$.^[25–28] To create the nanoarrays atop the Si pyramids, Ag nanoparticles were electrolessly deposited atop the Si pyramids, and the substrates were then subjected to 2 min of metal-assisted etching (MAE). During MAE, silicon is etched preferentially where the metal is located, producing nanowires atop the silicon pyramids.^[29]

Figure 2 shows the calculated and measured hemispherical (i.e., total) reflectance of a bare Si surface (black trace) and of the three structures of interest—microarrays (red trace), nanoarrays (blue trace), and hierarchical arrays (green trace). Upon first inspection, we note generally good agreement between the measured and simulated spectra with the exception of the nanoarrays' spectra, which we will return to discuss. For a more direct comparison, we averaged the hemispherical reflectance of these spectra from 300 to 2000 nm and report these averages in Table 1.

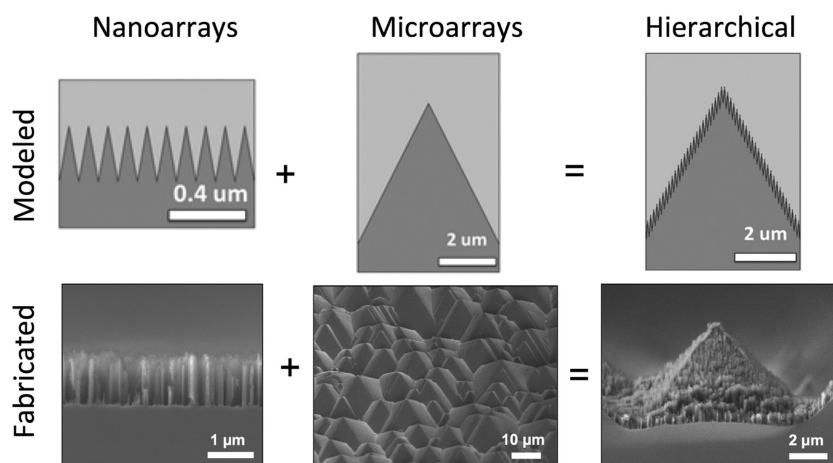


Figure 1. (Top row) Graphical representation of nanoarrays, microarrays, and hierarchical structures used in simulations, and (bottom row) corresponding scanning electron microscope images of fabricated structures.

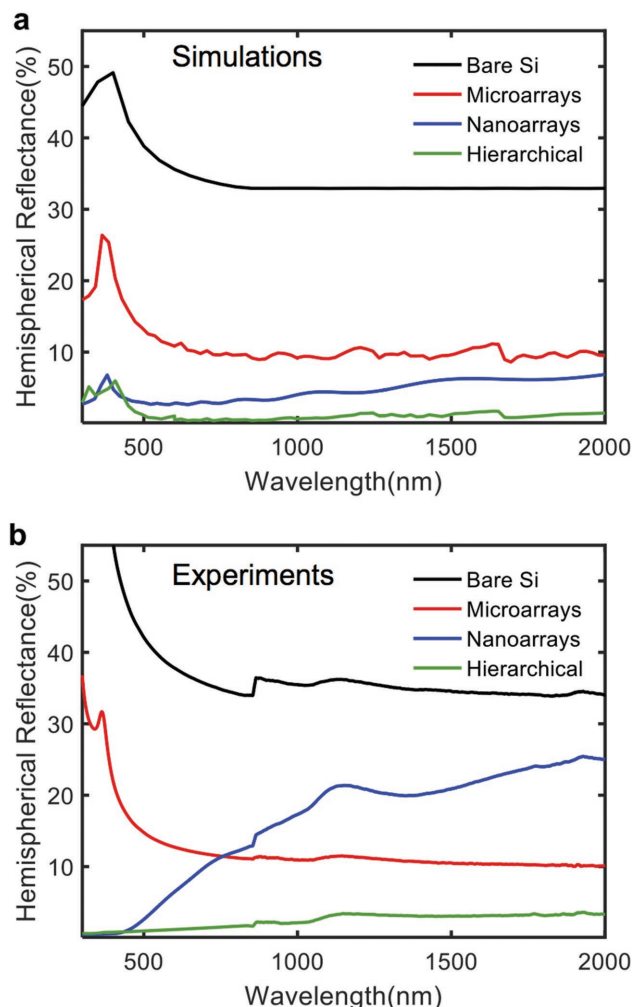


Figure 2. Hemispherical reflectance of bare silicon (black trace), microarrays (red trace), nanoarrays (blue trace), and hierarchical structures combining the micro- and nanoarrays (green trace) obtained from a) simulations using modeled structures and b) measurements of fabricated structures.

In agreement with others' experimentally reported values,^[19,26] we found that the average hemispherical reflectance of silicon decreases from 37.9% to 12.5% with pyramidal texturing; our simulations are closely matched, predicting that silicon's average reflectivity decreases from 34.9% to 10.9% with the introduction of microarrays. Such pyramidal microarrays alone are often used in the solar cell industry to reduce silicon's reflectance.^[25,26] However, by stacking nanoarrays atop the microarrays to create hierarchical structures, the total reflectance is yet further reduced to 2.4% by measurements and 1.3% by simulations across the solar spectrum. Incorporating such hierarchical structures into solar cells can thus increase solar cells' light absorption, potentially increasing their power conversion efficiency, as well.^[18,22,30,31]

Table 1. Measured and simulated reflectivity as a function of structure averaged from 300 to 2000 nm.

Structure	Avg. % hemispherical reflectance		Avg. % specular reflectance		Avg. % diffuse reflectance	
	Simulation	Experiment (AOI = 8°)	Simulation	Experiment (AOI = 5.1°)	Simulation	Experiment (AOI = 0°)
Silicon	34.9	37.9	34.9	31.4	0.0	0.3
Microarrays	10.9	12.5	1.8	0.3	9.1	13.0
Nanoarrays	4.7	16.1	4.7	10.5	0.0	1.5
Hierarchical	1.3	2.4	0.3	0.02	1.0	2.4

Returning to the spectra of the isolated nanoarrays depicted as the blue traces in Figure 2, we note poor agreement between the experiment- and simulation-derived results. Some discrepancy may stem from the fact that the simulations were performed with 2D structures, whereas the experimental data were collected from 3D structures. However, we believe that the primary origin for this disagreement stems from the fact that we modeled the fabricated nanowires as triangular. Compared to the fabricated nanowires, the modeled nanotriangles taper more and thus create a smoother transition in the effective refractive index of the textured layer. Nanowires with more tapered tips and thus more gradual changes in the effective refractive index have been shown to have lower reflectivity than straight-walled nanowires with blunt tips.^[9,12–17] We thus believe that our fabricated nanowires have a sharper change in the index of refraction at the nanowire-air interface than the modeled triangular-shaped wires and thus reflect more light.

It is interesting to note that, despite the disagreement between the measured and simulated hemispherical reflectance spectra of the isolated nanoarrays, the spectra of the hierarchical structures are still relatively closely matched. This observation points to another benefit of using hierarchical structures rather than simply using high-aspect ratio nanowires alone to reduce reflectance: the constraints on the nanoarray structures to achieve low (i.e., <5%) hemispherical reflectance appear to relax when the nanoarrays are stacked atop microarrays. However, if one wishes to reduce the reflectivity even further, then fine-tuning of the nanoarrays structures is likely necessary.

To better understand how the hemispherical reflectance spectra of the variously structured silicon surfaces can be fine-tuned, we also collected the nanoarrays', microarrays', and hierarchical structures' diffuse and specular reflectance. Specular reflectance occurs when light reflects at the same angle as the incoming light but mirrored with respect to the normal of the surface; polished, mirror-like surfaces have high specular reflectance. Conversely, diffuse reflectance occurs when light is scattered at multiple angles; matte but bright materials have high diffuse reflectance. The hemispherical or total reflectance of a surface is the sum of its diffuse and specular reflectance.

Table 1 also contains the average specular and diffuse reflectance from both measurements of our fabricated structures and simulations of our modeled structures. The sum of the measured diffuse and specular reflectance is close to but not exactly equal to the measured hemispherical reflectance, as it theoretically should be. We attribute this slight mismatch to differences in the experimental set-ups for the different types of reflectivity measurements that were not controllable. For example, the angle of incidence for the hemispherical, specular, and diffuse

measurements were 8°, 5.1°, and 0° from normal, respectively, and we did not have the ability to change the angle of incidence for the hemispherical or diffuse reflectance measurements.

By comparing the values of diffuse and specular reflectance for each type of surface structure, we can determine which type of reflectivity is the major contributor to the overall hemispherical reflectance. For example, all of a bare silicon wafer's hemispherical reflectance can be attributed to specular reflectance, which is consistent with it having a polished, mirror-like surface. When microarrays are introduced to the silicon surface, both measurements and simulations indicate that the specular reflectance drops to below 2% and that diffuse reflectance dominates. In contrast, nanoarrays by themselves demonstrate the opposite effect: their diffuse reflectance is low because these sub-wavelength structures are too small to scatter light and instead specular reflectance dominates.

Thus, as a general rule of thumb, our microarrays have relatively high diffuse reflectance and low specular reflectance, and oppositely, our nanoarrays have relatively low diffuse reflectance and high specular reflectance. Because the hemispherical or total reflectance is the sum of the diffuse and specular reflectance, it makes sense that combining these two types of arrays into hierarchical structures yields the lowest overall hemispherical reflectance. Interestingly, both measurements and simulations indicate that the diffuse reflectance is the primary contributor to the overall hemispherical reflectance of the hierarchical structures. Thus, if one wished to decrease the total hemispherical reflectance of hierarchical structures even further below 2%, this is most likely to be accomplished by focusing on decreasing diffuse reflectance.

We were interested to explore the structural parameter space of the nanoarrays to understand how the total hemispherical reflectance can further be reduced. Fortunately, the height of the nanowires can be easily increased simply by increasing the metal-assisted etching time. Figure 3a,b shows increasingly tall nanowires as a function of increasing etching time atop planar silicon and microarrays, respectively, which thereby allows us to study the effect of nanowire height on nanoarrays' and hierarchical structures' reflectivity. We collected the various reflectance spectra on all the samples. For an easier comparison across spectra, Figure 3c,d shows the average diffuse (left axis) and specular (right axis) reflectance as a function of nanowire height atop planar silicon (i.e., nanoarrays) and atop the pyramidal microarrays (i.e., hierarchical structures), respectively.

Focusing first on the nanoarrays by themselves, we observe that within 2 min of etching when the nanowires are no more than 1.1 μm tall, the diffuse reflectance increases slightly, which is consistent with some roughening of the previously

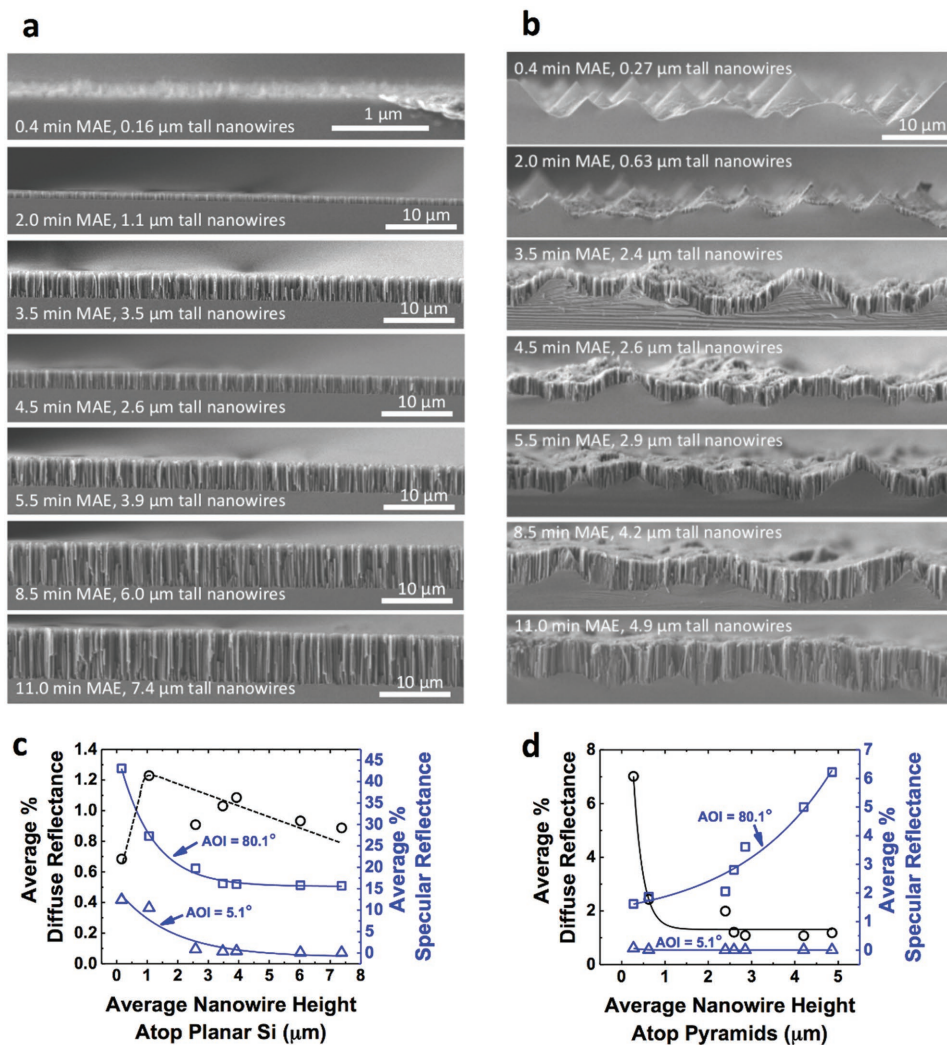


Figure 3. Scanning electron microscope images of a) Si wafers and b) Si pyramids (imaged at 90°) that have undergone MAE for the specified periods of time to form nanowires. In (b), scale bar is valid for all images. c,d) The diffuse (left axis, black open circles) and specular (right axis, blue symbols) reflectance averaged from 250 to 2500 nm as a function of the nanowire height atop c) planar Si and d) the pyramidal microarrays. The averaged specular reflectance collected at 5.1° (triangles) and 80.1° (rectangles) is shown. Solid lines are exponential decay or growth (as appropriate) fits to the data, whereas the dashed line is provided only as a guide for the eye.

polished wafer surface. However, as the nanowires increase in height with longer etching times, we observe that the diffuse reflectance actually decreases. We previously noted that the hemispherical (total) reflectance of our hierarchical structures that had undergone metal-assisted etching for 2 min was dominated by diffuse reflectance. That the diffuse reflectance of nanoarrays decreases with increasing nanowire height suggests that the hemispherical reflectance of hierarchical structures may be further decreased by using taller nanowires atop the microarrays.

Unlike the nonmonotonic decrease in the diffuse reflectance, the specular reflectance (blue symbols in Figure 3c) decreases exponentially with increasing nanowire height atop planar silicon. At near-normal incidence of 5.1°, the specular reflectance reaches values below <0.5% when the nanoarrays reach a height of ≈4 μm. However, the specular reflectance is significantly higher at higher angles of incidence; for example,

at 80.1°, the specular reflectance plateaus to ≈16%, which makes the surface still fairly reflective even by eye. Thus, while high-aspect ratio nanoarrays alone do significantly reduce a surface's reflectance, the antireflection properties they provide are not omnidirectional.

Having an understanding of how the height of structures affects the reflectivity of nanoarrays by themselves, we can now turn our attention to understanding how the height of nanoarrays incorporated into hierarchical structures affects their antireflective properties. While nanowires atop planar silicon showed a nonmonotonic decrease in diffuse reflectance with increasing nanowire height due to an initial roughening of the polished silicon surface, the microarrays underlying the hierarchical structure already provide a roughened surface. Thus, the diffuse reflectance of the hierarchical structures, characterized by the black trace in Figure 3d, decreases monotonically and exponentially with increasing nanowire height. The average

diffuse reflectance of the hierarchical structures decreases from 7.0% to 1.2% as the nanowires' heights increase from 272 nm to 4.86 μm , again demonstrating the benefit of having high-aspect nanowires.

Compared to the nanoarrays by themselves, the hierarchical structures have significantly lower specular reflectance, as might be expected given their underlying microarrays which effectively decrease specular reflectance. For example, at a 5.1° angle of incidence, the specular reflectance decreases exponentially from 0.07% when the nanowires are ≈ 272 nm tall and plateaus to $\approx 0.007\%$ once the nanowires are at least 1.5 μm tall (see blue triangles in Figure 3d). This exponential decrease with increasing nanowire height is similar to the trend observed for the nanowires by themselves atop planar silicon albeit that the magnitude of specular reflectance is significantly lower. However, interestingly, at high angles of incidence (e.g., $>65^\circ$), the specular reflectance of the hierarchical structures actually increases exponentially with increasing nanowires' height, as shown in by the blue squares in Figure 3d for an angle of incidence of 80.1° . We believe that this increase in the specular reflectance occurs because the underlying pyramidal microarrays are smoothed (i.e., their heights are reduced) during the extended etching times required to create taller nanowires. The flattening of the underlying pyramids with increasing nanowire height and etching time can be noticed in the scanning electron microscope (SEM) images of Figure 3b. The fact that we do not see a comparable increase in specular reflectance with increasing nanowire heights' on planar silicon also further supports this hypothesis. These results indicate that to create hierarchical structures with omnidirectional and ultralow hemispherical reflectance below 1%, it would be most desirable to grow high aspect ratio nanowires atop pyramidal microarrays rather than create the nanowires by etching into the pyramids as we have done here.

Having an understanding of how the height of the nanowires and pyramids each affect the hierarchical structures' overall reflectivity, we were next interested to understand how periodicity or lack thereof in the microarrays can affect reflectivity. As previously described, KOH-etching is a simple method for producing microarrays of pyramids in silicon (100) that reduce its specular reflectance, but the pyramids vary in size, making the structures aperiodic. Fabricating periodic pyramidal microarrays of varying geometries is possible but requires several extra patterning steps.^[18,20] Thus, to evaluate what potential benefits may be gained by tuning the periodicity of microarrays, we simulated pseudo-aperiodic microarrays and compared their reflectance against our simulation results from periodic microarrays discussed earlier consisting of triangles whose width and height are both 5 μm . We approximated aperiodic microarrays by including several triangles of varying sizes in a single cell, which was then repeated using periodic boundary conditions. Specifically, these pseudo-aperiodic microarrays consist of three triangles whose widths are 5, 2.3, and 7.7 μm (all with a 1:1 width:height ratio).

The specular and diffuse reflectance spectra of the periodic and aperiodic microarrays appear comparable below 1000 nm (see Figure S7, Supporting Information), but above 1000 nm where the wavelength is on the same length scale as the microarray structures, differences in the reflectance of the periodic

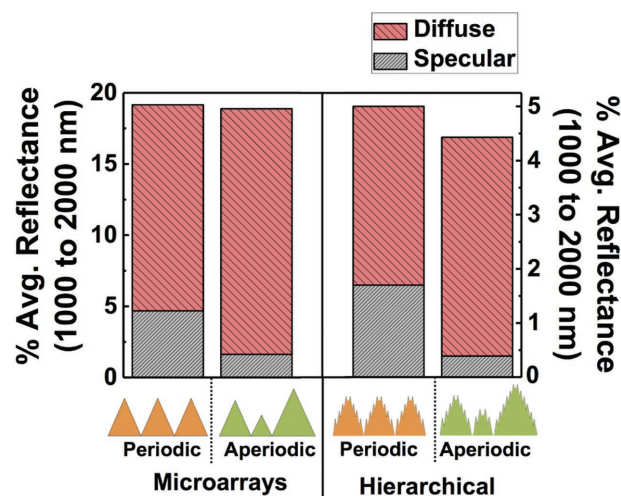
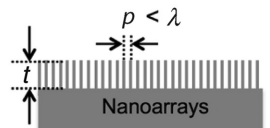
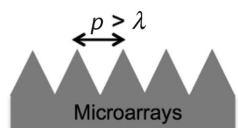
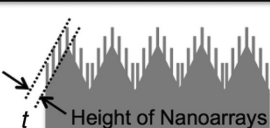
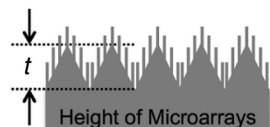
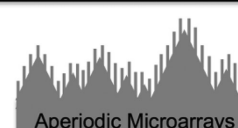


Figure 4. The average diffuse (pink) and specular (gray) reflectances, whose sum equals the hierarchical reflectance, in the near-IR regime of simulated periodic and aperiodic microarrays (left axis) and hierarchical arrays (right axis). The dimensions of the structures are described in the text.

and aperiodic microarrays become apparent. Focusing on this region of differences, the left axis in Figure 4 shows the specular and diffuse reflectance averaged from 1000 to 2000 nm of periodic and aperiodic microarrays. The average specular reflectance of the periodic microarrays is 4.7%, which is higher than the specular reflectance of the aperiodic microarrays at 1.6%. The higher specular reflectance of the periodic microarrays can be accounted for by diffraction effects, which occur when structures have a similar periodicity as the wavelength of light they interact with. The opposite trend holds for the diffuse reflectance: the average diffuse reflectance of the periodic microarrays at 14.5% is lower than that of the aperiodic microarrays at 17.3%. However, despite the differences in the specular and diffuse reflectance of the periodic and aperiodic microarrays, they still have comparable hemispherical reflectance (19.2% for periodic compared to 18.9% for aperiodic), which is the sum of the diffuse and specular reflectances.

We performed a similar analysis for hierarchical structures with underlying periodic and aperiodic microarrays, corresponding to the right axis in Figure 4. Atop both the periodic and aperiodic microarrays, we modeled nanoarrays consisting of smaller triangles with a 100 nm base and 677 nm height, the same as previously discussed. From Figure 4, we see that the magnitude of reflectance of the hierarchical structures is lower than the microarrays, but the same trend as observed for the microarrays still holds: hierarchical structures with aperiodic microarrays have decreased specular reflectance and increased diffuse reflectance compared to hierarchical structures with periodic microarrays, but the total hemispherical reflectance of the hierarchical structures with underlying periodic and aperiodic microarrays is comparable. Thus, it appears that the periodicity of the microarrays (or lack thereof) does not significantly affect the total hemispherical reflectance but does provide tunability over how much of the total reflectance is specular or diffuse. Greater periodicity results in higher specular reflectance and lower diffuse reflectance, while the opposite trend

Table 2. Summary of structural features' effects on reflectivity.

Structural Feature	Effect on Reflectivity
 <p>Nanoarrays</p>	$t > \approx 1 \mu\text{m} \propto \downarrow$ Diffuse reflectivity \downarrow Specular reflectivity
 <p>Microarrays</p>	\downarrow Specular reflectivity
 <p>Height of Nanoarrays</p>	$\uparrow t \propto \downarrow$ Diffuse reflectivity, especially at longer wavelengths
 <p>Height of Microarrays</p>	$\uparrow t \propto \downarrow$ Specular reflectivity, especially at high angles of incidence relative to normal
 <p>Aperiodic Microarrays</p>	\downarrow Periodicity $\propto \uparrow$ Diffuse reflectivity $\propto \downarrow$ Specular reflectivity when p is comparable to λ

holds with decreasing periodicity.^[32] This general rule, along with those already discussed, are graphically summarized in **Table 2**. Depending on the specific application of interest, it might be beneficial to use aperiodic arrays as a building block. For example, in solar cells it is beneficial to increase the diffuse transmission to relax angle dependency and increase the optical path, while in others (such as diffraction gratings) periodic hierarchical arrays will be the structure of choice to maintain the angle selectivity.^[33]

Using these experimentally and computationally derived rules of thumb, we optimized our fabrication scheme to produce silicon hierarchical structures with low hemispherical reflectance across the solar spectrum regardless of the angle of incidence of light, as would be of interest for solar cell applications. Because of the trade-off between decreasing diffuse reflectance and increasing specular reflectance with increasing nanowire height atop the flattened aperiodic pyramidal microarrays, the hierarchical sample with the lowest hemispherical reflectance is one that was etched for an intermediate amount of time (4.5 min), yielding nanowires that are $\approx 2.6 \mu\text{m}$ tall. **Figure 5a** shows the specular reflectance of this hierarchical structure for angles of incidence varying from 5.1° to 80.1° . The specular reflectance of these optimized hierarchical structures

remains below 1% even at angles as high as 67° , which would be beneficial for maximizing the light absorption of solar cells without active solar tracking.^[28]

The hemispherical reflectance spectrum of this sample is shown as the green trace in **Figure 5b**. Averaging the hemispherical spectrum from 250 to 2500 nm, this optimized hierarchical silicon structure has an average hemispherical reflectance of 1.1% and an averaged weighted reflectance of 1% using the ASTM G-173 standard from 280 to 2500 nm.^[34] The entire spectrum is below 2% reflectance, but two increases in reflectance are observable at ≈ 500 nm and 1100 nm. The increase in reflectance at ≈ 1100 nm is attributable to silicon's bandgap. We believe that the increase in reflectance at 500 nm is caused by photoluminescence, which has been shown to occur when silicon nanowires undergo nanoporosity during extended metal-assisted etching.^[28,35–37] Though this photoluminescence effectively increases the reflectance of such silicon hierarchical structures, it can be advantageous for solar cells as it provides a means of converting high energy UV and blue light to longer wavelengths where silicon-based solar cells operate more efficiently.^[28]

3. Conclusion

We explored the role that nanometer- and micrometer-scale substructures play in reducing the reflectivity of hierarchical structures that incorporate them, and in doing so, devised a set of guidelines for how details of the reflectivity can be fine-tuned. We found that the microarrays serve primarily to roughen the surface to decrease the specular reflectance over the range of incident angles. Contrastingly, the nanoarrays work effectively to decrease the diffuse reflectance and do so particularly well in the UV and visible wavelength regimes even with relatively short nanowire heights of $1 \mu\text{m}$ or less. In concert, these two features can be combined to create hierarchical structures that provide a remarkably low reflectance over a broad range of viewing angles (up to 80.1°) and wavelengths (250–2500 nm). Increasing the height of both nanoarrays and microarrays works to further decrease the diffuse and specular reflectance, respectively, and periodicity of the underlying microarrays can be used to fine-tune the ratio of specular and diffuse reflectance, as well as its angle-dependency. Using these guidelines and optimizing for the lowest total hemispherical reflectance, we fabricated hierarchical structures in silicon having an average hemispherical reflectance from 250–2500 nm of 1.1% and having specular reflectance $<1\%$ even at angles of incidence as high as 67° from normal. However, these guidelines can be used more broadly to fine tune reflective spectra of textured surfaces as required for various application needs.

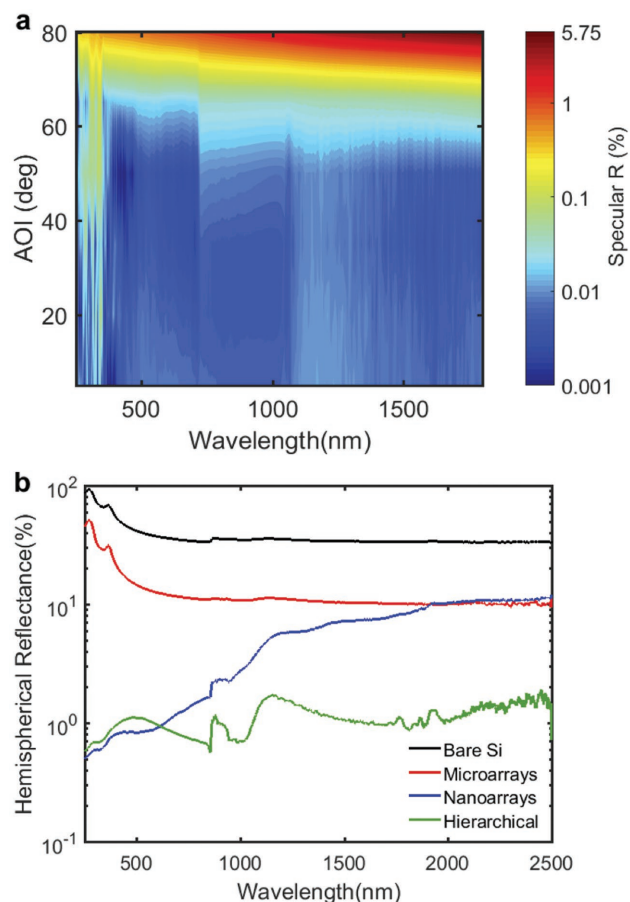


Figure 5. a) Measured specular reflectance (shown in log scale) at various angles of incidence (AOI) of our best hierarchical silicon structures, which consist of aperiodic pyramids with ≈ 2.6 μm tall nanowires on top. Spectra were attained at 5.1° , 20.1° , 35.1° , 50.1° , 65.1° , and 80.1° from normal and values in between are interpolated. b) Hemispherical reflectance of the same optimized hierarchical silicon structures as in (a) (green trace). The hemispherical reflectance of bare silicon (black trace), microarrays (red trace), and comparable nanoarrays consisting of ≈ 2.6 μm tall nanowires (blue trace) are provided for reference, as well.

4. Experimental Section

Simulations: COMSOL Multiphysics version 5.2a was used to simulate the structures of interest. A 2D simulation using the RF module was setup. Periodic boundary conditions were set on the sides to simulate an infinite array. Ports were used to create the input wave and to measure specular reflectance, while the overall reflectance was calculated by integrating the Poynting vector over the propagation direction. Diffuse reflectance was calculated by subtracting the specular reflectance from the hemispherical reflectance. Transverse electric waves with the E-field normal to the plane of incidence were used. A combination of perfectly matched layers and second-order scattering boundary conditions was used to minimize any reflections related to the finite area of the simulation setup. The refractive index of silicon was extracted from Palik.^[38] The extinction coefficient was not included in the simulations to separate any bulk silicon effects and analyze only the reflectance (reflectivity related to the surface and not to the bulk) for a more general result.

Sample Fabrication: P-type boron-doped Si (100) wafers with 0.0100–0.0180 Ω cm resistivity (Addison Engineering, San Jose, CA) were used for all sample fabrication. Wafers were used straight from the box

without any precleaning. A solution consisting of 500 mL deionized water, 55.6 mL isopropanol alcohol (10 vol%), and 12.8 g dissolved KOH pellets (2.3 wt%) was heated to 70°C . Si wafers were placed face-up in the beaker of heated solution for 40–60 min until the surface was uniformly antireflective. The resulting pyramids had an average pitch of 5.2 ± 3.3 μm and an average etching angle of $59.8^\circ \pm 1.3^\circ$, resulting in comparable pitch and height. We found that placing samples face-up reduced defects in the surfaces caused by bubble formation. We followed the recipe used by Qi et al.^[19] for electroless deposition of Ag, which involved dipping substrates in a room-temperature solution of 4.9 M HF solution with 0.01 M AgNO_3 for $\approx 30 \pm 5$ s. Figure S1 (Supporting Information) shows Si pyramids after Ag deposition. Samples were immediately rinsed with deionized water, dried with nitrogen, and then subjected to MAE.

Using the metal-assisted etching recipe provided by Qi et al.^[19] yielded pitted structures rather than nanowires, as shown in Figure S2 (Supporting Information). Wafers' doping type and doping concentrations are known to affect the types of structures formed by MAE carried out under otherwise identical conditions,^[29] and it was believed that a difference in the type of wafers used in this study and in Qi et al. accounted for unexpected structures when following the recipe of Qi et al.^[19] Qi et al. used *n*-type wafers, whereas this study used *p*-type wafers. However, nanostructures formed by MAE are also known to vary significantly based on the concentration of HF and H_2O_2 . Chartier et al. found that higher concentrations of HF relative to H_2O_2 produced more wire-like structures and lower concentrations of HF relative to H_2O_2 produced more pitted structures like those that were seen when following the recipe of Qi et al.^[29,39] Thus, the volume ratio of 49% HF to 30% H_2O_2 to water was changed to 2:1:8.5 (40 mL 49% HF, 20 mL of 30% H_2O_2 , and 170 mL deionized water), and indeed, MAE with this solution created yielded more wire-like structures with the substrates that were comparable to those attained by Qi et al.^[19] Ag-coated samples were placed face-up in a beaker of this room-temperature solution for 0.4–11 min, and subsequently rinsed with deionized water and dried with nitrogen. Remaining Ag was removed by dipping samples for 2 min in nitric acid, and again samples were rinsed with deionized water and dried with nitrogen.

Reflectance Measurements: Diffuse and hemispherical reflectances were collected on a PerkinElmer Lambda 950 spectrometer with 60 mm integrating sphere. Diffuse and hemispherical reflectance measurements were performed with the light incidence at 0° and 8° , respectively, relative to the substrate normal, and these spectra were collected from 250 to 2500 nm in 1 nm intervals with 0.2 s detector integration times. Spectra were smoothed to enhance the signal-to-noise ratio (SNR) by averaging every 10 adjacent data points (i.e., “box-car smoothing”). Specular reflectances from 250 to 1800 nm were collected on an Agilent Cary 6000 spectrometer equipped with Agilent's universal measurement accessory for measuring specular reflectance at variable angles. Spectra were collected in 1 nm intervals and with 0.1 s detector integration times for incident light angles of 5.1° , 20.1° , 35.1° , 50.1° , 65.1° , and 80.1° relative to the substrate normal. These spectra were likewise smoothed by averaging every 10 adjacent data points to enhance the SNR. FTIR reflectance measurements were taken using a Vertex 70 FTIR instrument (Bruker Optics, Billerica, MA) in the 2.5–20 μm range. Specular reflectivity was measured at an 11° angle of incidence. The data were normalized with respect to a gold standard.

Supporting Information

Supporting Information is available from the Wiley Online Library or from the author.

Acknowledgements

J.J.D.L. and A.M.H. contributed equally to this work. This work was performed under the auspices of the U.S. Department of Energy by

Lawrence Livermore National Laboratory under Contract No. DE-AC52-07NA27344. Funding was provided through Lab Directed Research Development (LDRD) 15-ERD-043. LLNL-JRNL-713005.

Conflict of Interest

The authors declare no conflict of interest.

Keywords

broadband and omnidirectional antireflectivity, hierarchical structures, silicon

Received: January 24, 2017

Revised: February 23, 2017

Published online:

- [1] Y.-F. Huang, S. Chattopadhyay, Y.-J. Jen, C.-Y. Peng, T.-A. Liu, Y.-K. Hsu, C.-L. Pan, H.-C. Lo, C.-H. Hsu, Y.-H. Chang, C.-S. Lee, K.-H. Chen, L.-C. Chen, *Nat. Nanotechnol.* **2007**, *2*, 770.
- [2] S. Yalamanchili, H. S. Emmer, K. T. Fountaine, C. T. Chen, N. S. Lewis, H. A. Atwater, *ACS Photonics* **2016**, *3*, 1854.
- [3] S. K. Srivastava, D. Kumar, P. K. Singh, M. Kar, V. Kumar, M. Husain, *Sol. Energy Mater. Sol. Cells* **2010**, *94*, 1506.
- [4] K. T. Fountaine, W.-H. Cheng, C. R. Bukowsky, H. A. Atwater, *ACS Photonics* **2016**, *3*, 1826.
- [5] G. Gervinskas, G. Seniutinas, J. S. Hartley, S. Kandasamy, P. R. Stoddart, N. F. Fahim, S. Juodkakis, *Ann. Phys.* **2013**, *525*, 907.
- [6] J. Cai, L. Qi, *Mater. Horiz.* **2015**, *2*, 37.
- [7] K.-C. Park, H. J. Choi, C.-H. Chang, R. E. Cohen, G. H. McKinley, G. Barbastathis, *ACS Nano* **2012**, *6*, 3789.
- [8] Q. Y. Yang, X. A. Zhang, A. Bagal, W. Guo, C. H. Chang, *Nanotechnology* **2013**, *24*, 235202.
- [9] A. Rahman, A. Ashraf, H. Xin, X. Tong, P. Sutter, M. D. Eisaman, C. T. Black, *Nat. Commun.* **2015**, *6*.
- [10] L. Chan, D. Kang, S.-M. Lee, W. Li, H. Hunter, J. Yoon, *Appl. Phys. Lett.* **2014**, *104*.
- [11] M. L. Brongersma, Y. Cui, S. Fan, *Nat. Mater.* **2014**, *13*, 451.
- [12] Z. Diao, M. Kraus, R. Brunner, J. H. Dirks, J. P. Spatz, *Nano Lett.* **2016**, *16*, 6610.
- [13] S. Ji, J. Park, H. Lim, *Nanoscale* **2012**, *4*, 4603.
- [14] J.-Y. Jung, Z. Guo, S.-W. Jee, H.-D. Um, K.-T. Park, J.-H. Lee, *Opt. Express* **2010**, *18*, A286.
- [15] B. Hua, B. Wang, M. Yu, P. W. Leu, Z. Fan, *Nano Energy* **2013**, *2*, 951.
- [16] J. Zhu, Z. Yu, G. F. Burkhard, C.-M. Hsu, S. T. Connor, Y. Xu, Q. Wang, M. McGehee, S. Fan, Y. Cui, *Nano Lett.* **2009**, *9*, 279.
- [17] Y. F. Huang, S. Chattopadhyay, *J. Nanophotonics* **2013**, *7*, 073594.
- [18] R. Tasmiat, N.-C. Miguel, F. Kristel, *Nanotechnology* **2014**, *25*, 485202.
- [19] D. Qi, N. Lu, H. Xu, B. Yang, C. Huang, M. Xu, L. Gao, Z. Wang, L. Chi, *Langmuir* **2009**, *25*, 7769.
- [20] B. D. Choudhury, A. Abedin, A. Dev, R. Sanatinia, S. Anand, *Opt. Mater. Express* **2013**, *3*, 1039.
- [21] B. Dudem, J. W. Leem, J. S. Yu, *RSC Adv.* **2016**, *6*, 3764.
- [22] Y. Liu, A. Das, Z. Lin, I. B. Cooper, A. Rohatgi, C. P. Wong, *Nano Energy* **2014**, *3*, 127.
- [23] S. J. Cho, T. An, G. Lim, *Chem. Commun.* **2014**, *50*, 15710.
- [24] C.-H. Chang, J. A. Dominguez-Caballero, H. J. Choi, G. Barbastathis, *Opt. Lett.* **2011**, *36*, 2354.
- [25] I. Zubel, *Sens. Actuators, A* **2000**, *84*, 116.
- [26] D. L. King, M. E. Buck, presented at 22nd IEEE Photovoltaic Specialists Conf., Las Vegas, NV, October **1991**.
- [27] Y. Fan, P. Han, P. Liang, Y. Xing, Z. Ye, S. Hu, *Appl. Surf. Sci.* **2013**, *264*, 761.
- [28] T. Dzhaferov, *Silicon Solar Cells with Nanoporous Silicon Layer, Solar Cells - Research and Application Perspectives*, (Ed: A. Morales-Acevedo), InTech, Rijeka, Croatia **2013**.
- [29] Z. Huang, N. Geyer, P. Werner, J. de Boor, U. Gösele, *Adv. Mater.* **2011**, *23*, 285.
- [30] X. Liu, P. R. Coxon, M. Peters, B. Hoex, J. M. Cole, D. J. Fray, *Energy Environ. Sci.* **2014**, *7*, 3223.
- [31] S. Thiyagu, C.-C. Hsueh, C.-T. Liu, H.-J. Syu, T.-C. Lin, C.-F. Lin, *Nanoscale* **2014**, *6*, 3361.
- [32] T. A. Germer, *J. Opt. Soc. Am. A* **2007**, *24*, 696.
- [33] E. Yablonovitch, *J. Opt. Soc. Am.* **1982**, *72*, 899.
- [34] C. A. Gueymard, D. Myers, K. Emery, *Sol. Energy* **2002**, *73*, 443.
- [35] A. G. Cullis, L. T. Canham, *Nature* **1991**, *353*, 335.
- [36] A. G. Cullis, L. T. Canham, P. D. J. Calcott, *J. Appl. Phys.* **1997**, *82*, 909.
- [37] L. T. Canham, *Appl. Phys. Lett.* **1990**, *57*, 1046.
- [38] *Handbook of Optical Constants of Solids* (Ed: E. D. Palik), Elsevier, Amsterdam, The Netherlands **1997**.
- [39] C. Chartier, S. Bastide, C. Lévy-Clément, *Electrochim. Acta* **2008**, *53*, 5509.